

Fracture Behavior of Woven Silicon Carbide Fibers Exposed to High-Temperature Nitrogen and Oxygen Plasmas

Walten Owens, Daniel Merkel, Frederic Sansoz,[†] and Douglas Fletcher[†]

Mechanical Engineering Program, School of Engineering, The University of Vermont, Burlington, Vermont 05405

High-temperature aero-thermal heating in a 30 kW inductively coupled plasma torch was used to replicate the effects of harsh oxidizing environments during hypersonic atmospheric entry on fracture behavior and microstructure of two-dimensional woven SiC fibers. Hi-Nicalon SiC woven cloths were exposed to surface temperatures over 1400°C with different high-enthalpy dissociated oxygen and nitrogen plasma flows, and were subsequently deformed in pure tension at room temperature. Changes in fiber microstructure and surface chemistry after thermal exposure were examined by scanning electron microscopy. Pure nitrogen plasmas resulted in a 50% decrease of strength in woven SiC fibers with minimal effects on the fiber structure, except for highly localized surface pitting caused by partial decomposition of silicon oxycarbonitride phase at high temperature. In contrast, exposure to dissociated oxygen and air plasmas led to severe strength reduction and embrittlement over significantly short time scales, corresponding to degradation rates up to 200 times higher than those reported with static heating at equivalent temperatures. The origin of accelerated embrittlement at microscopic scale was found related to complex gas-surface interactions and high-temperature oxidizing processes involving the formation of SiO₂ bubbles and microcracks on the surface. These findings are important for the development of outer fabric materials for new flexible thermal protection systems in space applications.

I. Introduction

INFLATABLE aerodynamic decelerators (IAD) are being developed as a deployable alternative to conventional rigid thermal protection systems for mitigating the aero-thermal heating associated with atmospheric entry on earth and other planets.¹ A critical component of the inflated structure is an outer fabric material that must withstand intense post-shock heating and highly reactive air plasmas, while remaining strong and elastically compliant to accommodate the associated stresses of flight. Two-dimensional (2-D) woven SiC fibers such as commercially available Hi-Nicalon fibers, are promising outer fabric materials owing to their excellent flexibility and high-temperature resistance.¹ However, our current understanding of deformation and failure behavior in 2-D woven SiC fibers exposed to high-enthalpy dissociated gas flows is limited. Extensive thermal testing on SiC fibers has been performed in static heating environments or by flowing molecular gases in more conventional furnaces,^{2–23} but these test configurations are far from the actual conditions of flight. Convective heating from flowing dissociated gases accompanied by radiation is more representative of hypersonic flight aerothermodynamics, and this environment

could significantly enhance chemical reactions at surfaces in SiC.²⁴ Therefore, the objective of the present study is to examine the performance of 2-D woven SiC fibers in an aero-thermal environment that better replicates the conditions of atmospheric trajectory heating, using a 30 kW inductively coupled plasma (ICP) torch, with a particular focus on understanding the influence of plasma chemistry and surface temperature on fabric strength. This study demonstrates that oxidizing plasmas play a more detrimental role on fracture strength of 2-D woven SiC fibers than conventional static heating at equivalent temperatures.

II. Experimental Methods

(1) Materials

Hi-Nicalon woven SiC fibers (COI Ceramics, Inc, South Magna, UT) were used in this study. The microstructure of these fibers is comprised of β -SiC nano-crystals that are separated by intergranular free carbon and a silicon oxycarbide phase.² The heterogeneous fiber has a Si:C:O weight percentage ratio of 62:37:0.5, respectively, with less than 0.3% hydrogen remaining from the organo-silicon precursor. The small oxygen incorporation in the molecular structure could lead to thermal instability and poor oxidation resistance. Alternatively, purely stoichiometric SiC fibers contain less oxygen,³ but this type of fiber exhibits poor flexural strength.¹

The SiC fibers in the present study were distributed in the form of tows, which were untwisted bundles of parallel, continuous filaments as shown in Fig. 1(a). The SiC tows were woven together to form a cloth, Figs. 1(b) and (c). To minimize fiber to fiber abrasion, the tows were coated with a poly vinyl alcohol coating.²⁵ A 5 harness satin weave was studied as it was determined to be advantageous due to its limited permeability and ability to conform to complex curves.¹ This weave type presented 26 fibers per inch in both the warp and weft directions, with each fiber overlapping 4 cross fibers before being woven under 1 cross fiber. The filaments within tows conformed to a lenticular shape due to the crimp of the weave. Some gap between the fibers allowed for gas-surface interactions to take place around the circumference of individual filaments.

(2) Aero-thermal Testing

20-mm diameter coupons were made by mechanically punching a sheet of SiC fabric. The fabric coupons had a bulk thickness of 0.5 mm and an average mass of 0.14 g. An electrically insulated sting arm holding the coupons at a fixed position was used to quickly insert the samples into an already established plasma stream. The mounting apparatus shown in Fig. 1(c), developed in collaboration with the NASA Langley research center, used a clasp design that held the coupon in the center of a 25 mm outer diameter sintered SiC sleeve. The secured outer edges of the coupon limited the actual exposed diameter to 18 mm while providing an edge chamfer of 3 mm radius for the overall sample holder. This was done to ensure that the velocity gradient over the fabric

N. Jacobson—contributing editor

Manuscript No. 36911. Received May 15, 2015; approved July 13, 2015.

[†]Author to whom correspondence should be addressed. e-mails: frederic.sansoz@uvm.edu, douglas.fletcher@uvm.edu

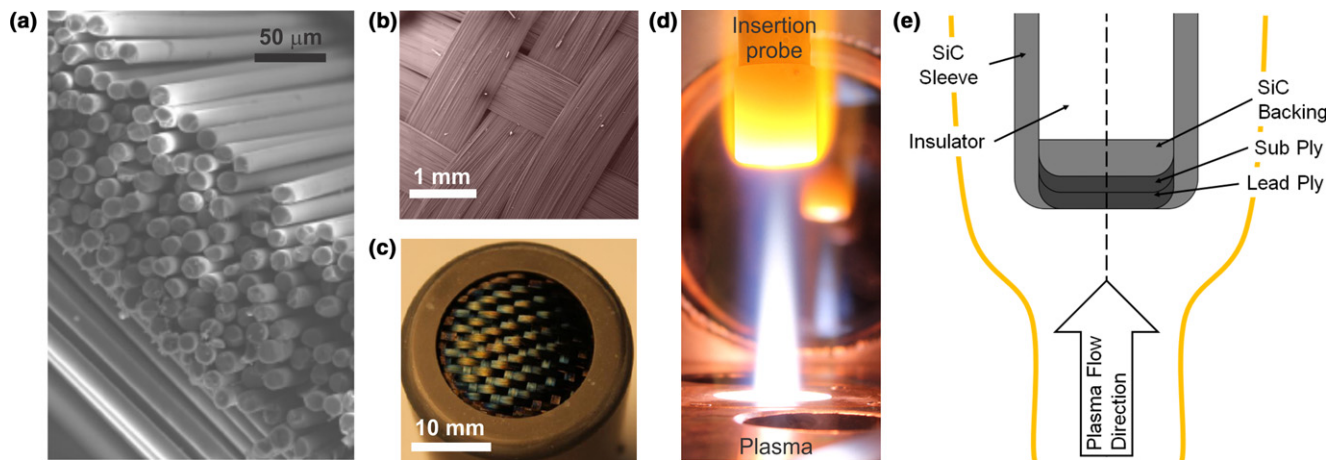


Fig. 1. Aerothermal testing of 2-D woven SiC fibers. (a) Cross-sectional and (b) top views of woven SiC fibers by SEM. (c) Woven Hi-Nicalon SiC lead-ply coupon in SiC sleeve. (d) Probe insertion in the 30 kW inductively coupled plasma torch facility. (e) Schematic illustration of a longitudinal cross-section view of the insertion probe.

samples was the same as that over the facility heat flux probe. A sintered SiC backing piece was used behind the coupons and was contoured to provide a smooth and flush surface between the coupon and the sleeve edge.

Two outer fabric coupons were tested simultaneously similar to the lead-ply and sub-ply structure used in IAD. The lead-ply coupon was exposed directly to the plasma flow while the sub ply was mildly protected between the lead ply and the SiC backing piece. To limit conduction losses, a refractory insulator (ZIRCAR RSLE-57, ZIRCAR Refractory Composites, Inc., Florida, NY) was used to thermally isolate the coupon from the rest of the insertion probe. A profile view of the ICP test configuration is displayed in Figs. 1(d) and (e). Aerothermal conditions tested in this work included 100% nitrogen, dilute air, normal air, and 100% oxygen plasmas at a constant chamber static pressure of 160 torr. The operating conditions for each test including flame temperature and mixture are presented in Table I.

(3) *In-Situ Surface Temperature and Emission Measurements*

A central hole through the holder components provided thermocouple access to measure sub-ply temperatures. Surface temperatures for the lead ply were recorded using a Marathon Series (Raytek, Santa Cruz, CA) MR1SACF and MR1SCCF infrared pyrometer (600°C–3000°C range) operating with a 0.75–1.1 μm wavelength range. Despite the temporal variations in surface temperature due to the catalytic and reactive heating that is specific to the plasma chemistry, operating conditions were chosen to provide similar steady state temperatures for all gases. Figure 2 shows that the

samples tested in pure air and air-nitrogen plasmas attained relatively constant surface temperatures within $\pm 25^\circ\text{C}$ after 5 s. In pure nitrogen plasma, phase transformation of the fibers at high temperature and the absence of additional heating from dissociated oxygen required exposure up to 1 min before achieving a constant surface temperature, as discussed below. In pure oxygen plasma, we observed some high-temperature excursions due to surface flares appearing in the video records, as shown in inset of Fig. 2. However, surface temperatures remained constant outside these excursions, and therefore were considered inconsequential for the temperature analysis.

It is important to note that in ICP torch experiments, the achievable surface temperatures were bounded by the minimum power of the torch at low temperatures and the catastrophic failure of the cloths at higher heat fluxes and temperatures. In Table I, the temperature of test B1 was estimated at 726°C based on thermocouples placed between the lead-ply and sub-ply coupons. Due to the inability to accurately measure the SiC surface temperatures below 1200°C using the pyrometer in 2 color mode, 1 color mode was used with an emissivity set at 0.6. The uncertainty in temperature measurements primarily resulted from a combination of errors from the thermocouples and the pyrometer.

An Ocean Optics HR-4000 (Ocean Optics, Dunedin, FL) series emission spectrometer was used to make temporally resolved measurements of the plasma flow emission, which can provide a qualitative indication of chemical activity, in front of the samples. Mirrors located approximately 60 cm from the plasma axis formed a conical collection envelope across the entire material surface and reflected the emission into an Ocean Optics P400-2-UV-VIS fiber optic cable

Table I. ICP Torch Operating Conditions for Aerothermal Testing. Tests A1–A4 were Used to Characterize the Effects of Plasma Environment, and Tests B1–B4 for the Effects of Surface Temperature

Sample	Plasma conditions			Temperature ($^\circ\text{C}$)		
	Gas mixture	Gas flow slpm, ($\pm 10\%$)	Power, kW (± 2 kW)	Heat flux, W/cm^2 ($\pm 15\%$)	Lead ply ($\pm 50^\circ\text{C}$)	Sub ply ($\pm 75^\circ\text{C}$)
A1	Nitrogen	40	14	62	See Fig. 2	
A2	Air: Nitrogen	15: 30	14	73	See Fig. 2	
A3	Air	40	14	80	See Fig. 2	
A4	Oxygen	40	12	79	See Fig. 2	
B1	Oxygen: Argon	10: 30	3.7	26	846	726 [†]
B2	Oxygen: Argon	10: 30	6.6	57	1262	1142
B3	Oxygen: Argon	10: 30	7.5	78	1420	1300
B4	Oxygen: Argon	10: 30	10.3	107	1533	1413

[†]($\pm 10^\circ\text{C}$) error.

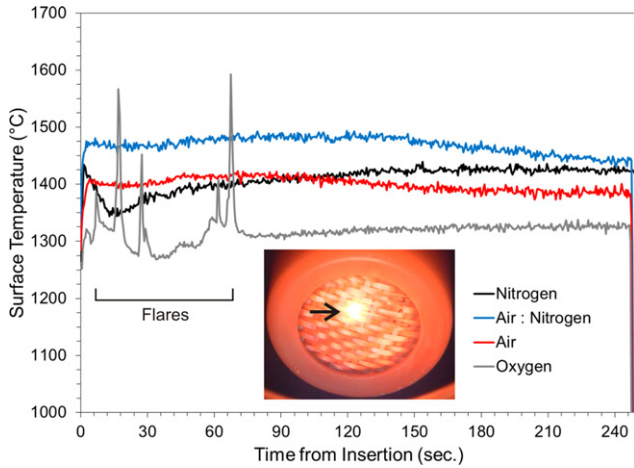


Fig. 2. Two-color pyrometer measurements of coupon surface temperature for tests in different plasma gases. Inset shows a snapshot taken from an *in-situ* video recording device during a surface flare in oxygen plasmas.

(Ocean Optics) attached to the spectrometer, which was operated between 200 and 1100 nm with a spectral resolution of 0.27 nm. The fiber optic cable was rated for wavelengths between 300 and 1100 nm. This wavelength range allowed for the detection of N atom, O atom, CN, NO and N₂ as well as silicon carbide (SiC) oxidation products such as Si, SiO, and SiO₂.

(4) Microstructure and Mechanical Characterization

Microstructure characterization of virgin and plasma-treated woven SiC fibers was conducted by secondary-electron scanning electron microscopy (SEM, JEOL, Peabody, MA) and standard optical microscopy. Semiquantitative elemental characterization was obtained using an energy dispersive x-ray microanalysis system (EDS) inside the SEM.

Tensile tests at room temperature with a materials testing machine (Test Resources 1000M single column tensile testing machine equipped with a 5-kN capacity force transducer, Test Resources, Inc., Shakopee, MN) were performed on coupons following plasma exposures of 30, 60, 120, and 240 s. Due to the circular shape of the coupons, metal pipe strapping was attached at the opposite ends using a two-part adhesive to securely mount the specimen in the grips, as shown in Fig. 3(a). A custom-made mounting jig was used to ensure a consistent gage length of 6 mm and to limit any

off-axis loading to $\pm 5^\circ$. The tensile strength of fabric materials can differ between warp and weft directions,⁴ but visually distinguishing the weave direction in the coupons was not possible. However, because of the asymmetry of the satin weave, which made the fibers on one face run in one direction, we always oriented the loading direction in the run direction on the windward side. For each test, an average of 18 tows were subjected to a load, leaving approximately 4–6 tows unattached for the specified gage length, as illustrated in inset of Fig. 3(a). Tensile deformation was carried out at a constant displacement rate of 1 mm/min until fracture occurred, as depicted in Fig. 3(b). In the results below, we have excluded all tests that did not fail within the gage length. Also a minimum of three tests were conducted at each condition in order to estimate the statistical strength distribution.

Figure 3(a) displays a representative load-displacement curve showing that the cloth deformation is quasi-linear with a clean break at peak load F_{\max} . The fracture strength σ_f was estimated by using

$$\sigma_f = \frac{F_{\max}}{\pi f(D/2)^2}, \quad (1)$$

where f is the total number of failed fibers, and D is the average fiber diameter. f was determined by counting the total number of broken tows times the average number of fibers per tow. Using SEM analysis, we found $D \sim 14 \mu\text{m}$ and an average of 500 fibers per tow. No significant change in fiber diameter was detected from SEM inspections during the transition from SiC to SiO₂, possibly due to the short exposure times considered in this study. Uncertainty in fracture strength measurements was included by counting the number of attached tows before and after the tensile test to take into account tows de-bonded from the adhesive in the grips.

III. Results and Discussion

(1) Exposure to Nitrogen Plasma

Figure 4 presents the emission spectra within the thermal boundary layer upon insertion in nitrogen or air plasmas. This figure shows evidence of gas-surface interactions in nitrogen plasma through strong CN emission immediately after insertion that quickly tapered off after 30 s. Depletion of Si and C species was detected in the form of C₂ and atomic Si emission within the first few seconds, but this phenomenon was absent during insertion in air plasma. The latter could be attributed to the removal of free carbon from thermal decomposition of silicon oxycarbide phase, which is

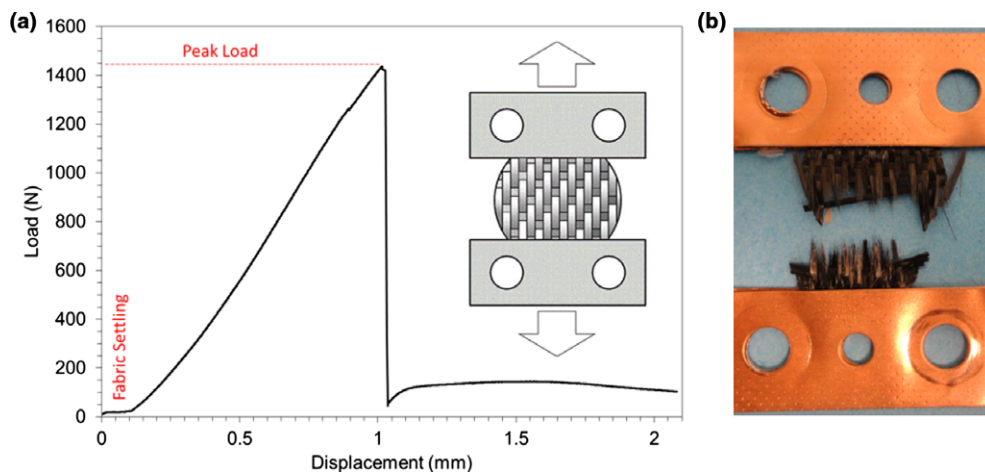


Fig. 3. Tensile testing of 2-D woven SiC fibers. (a) Representative load-displacement curve showing a clean break at peak load. Inset shows the yarn orientation with respect to the loading direction. (b) Coupon after fracture.

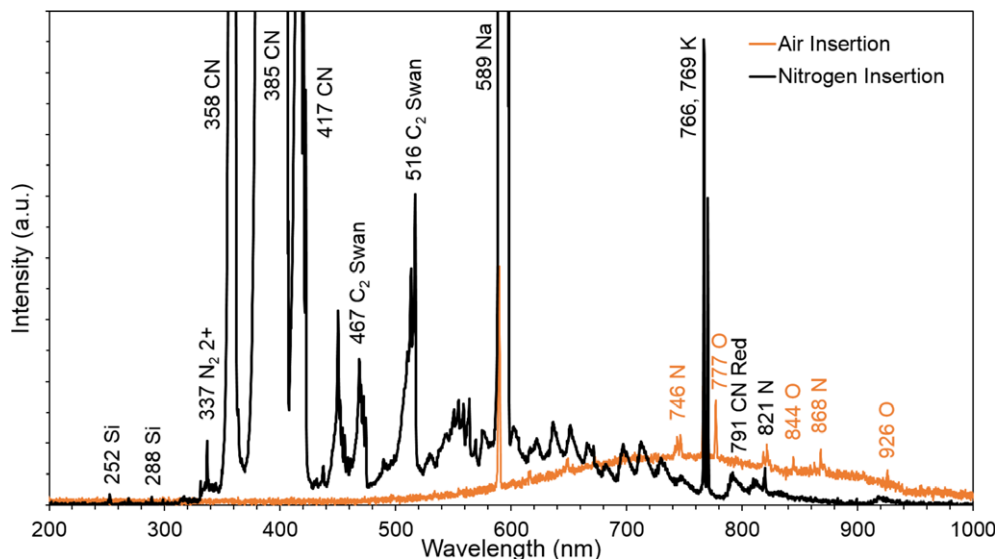


Fig. 4. Emission within the thermal boundary layer (~ 3 mm) upon insertion in air and nitrogen plasmas. Emission spectra collected using an integration time of 10 s at a location less than 3 mm away from the SiC surface immediately after insertion.

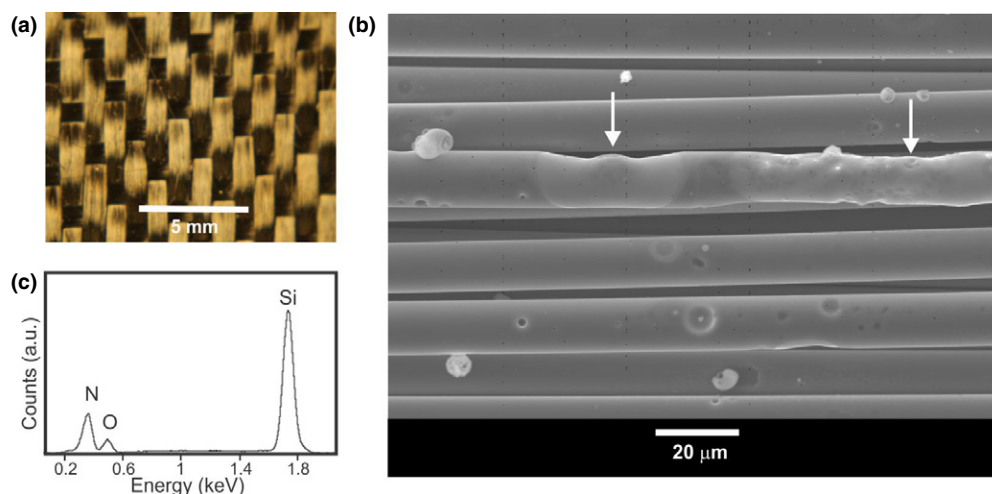


Fig. 5. Structure of 2-D woven SiC fibers after pure nitrogen plasma exposure for 240 s. (a) Optical micrograph and (b) SEM image of the exposed lead-ply surface. (c) EDS results from damaged locations indicated by arrows.

initially present between the grains, giving place to the formation of β -SiC.⁵ However, the optical micrograph presented in Fig. 5(a) shows no significant surface discoloration after nitrogen plasma exposure, which suggests that neither significant composition change nor thin-film formation took place on the fiber surface.

Furthermore, Fig. 5(b) shows a SEM image of the lead-ply surface after exposure, revealing that the SiC fibers remained smooth in nitrogen plasmas, like the microstructure of virgin fibers in Fig. 1(a). A few fibers did present localized surface damage in the form of pitting and fiber thinning, as indicated by arrows in Fig. 5(b). The EDS analysis in Fig. 5(c) shows evidence for significant concentrations of nitrogen and oxygen in the damage locations. This result agrees with the possible formation of stable $\text{Si}_2\text{N}_2\text{O}$ phase at temperatures between 1400°C and 1800°C in the Si–C–N–O system for low oxygen concentrations.^{26,27} Likewise, during static heating of Hi-Nicalon SiC fibers in pure nitrogen environment, Shimoo et al. noted the growth of an equilibrium surface layer rich in oxygen and nitrogen attributed to silicon oxycarbonitride phase at 1300°C , but also full decomposition of this phase after re-heating up to 1600°C .⁵ Therefore, it is possible to assume that the highly localized pitting of the fibers in Fig. 5(b) could result from a partial decomposition of silicon oxycarbonitride phase, since the

temperature range explored here was between 1350°C and 1400°C (Fig. 2), i.e. between the two extreme conditions tested by Shimoo et al.

Figure 6 represents the room-temperature fracture strength of coupons subjected to partially dissociated nitrogen plasma at different times of exposure. Comparatively, the average strength for virgin coupons in the present study was found to be half the tensile strength of individual Hi-Nicalon fibers reported in the literature.⁵ This pronounced weave effect on fracture strength can be interpreted from fiber to fiber abrasion and weaving damage that could counteract the potential increase in strength due to the fabric assistance provided by the weave.²⁸ Moreover, a past study on the tensile strength of single tows and single filaments has suggested an approximate 40% loss in strength when multiple filaments are tested simultaneously, due to the stochastic nature of brittle failure in ceramic fiber bundles.⁶

Figure 6 shows that the fracture strengths of both lead-ply and sub-ply coupons decrease dramatically after seconds of exposure in nitrogen plasmas, but appears to level off at a 50% strength reduction, from 1.7 GPa down to ~ 0.85 GPa, for durations above 30 s. It is also worth mentioning that coupons exposed to longer exposure times over 40 min were found to retain their structural integrity. After any rapid transient effects that occur within 30 s, a constant strength

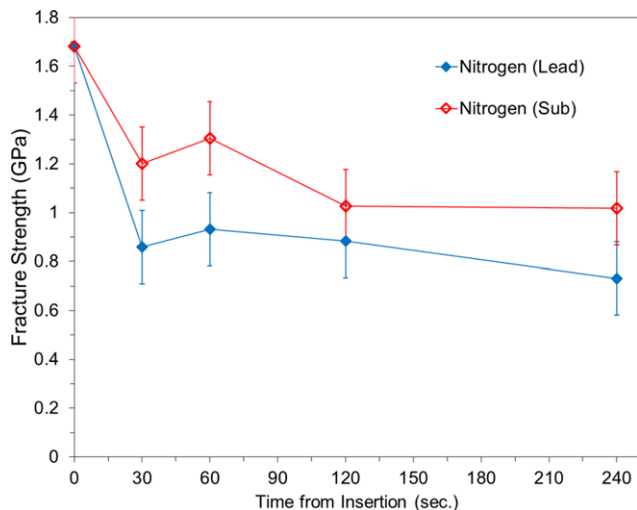


Fig. 6. Room-temperature fracture strength of the lead-ply and sub-ply coupons after exposure to nitrogen plasma. The virgin material strength before exposure or time zero was averaged over 3 tests.

offset between lead-ply and sub-ply coupons was observed. The larger strength retention of the sub-ply coupon may have arisen from the naturally lower temperatures behind the lead ply, which may have limited the occurrence of phase transformations at high temperature.

In static heating, microstructural changes from thermal decomposition of amorphous silicon oxycarbide phase at high temperatures has been commonly reported to explain the fiber strength reduction in non-stoichiometric SiC fibers.^{2,5,7-9} Shimoo et al.⁵ observed a ~50% decrease in tensile strength of single Hi-Nicalon fibers after heat-treatment in nitrogen up to 1600°C, which was related to the formation of micropores on the fiber surface as a result of thermal decomposition of the silicon oxycarbonitride phase. Therefore, the fracture behavior of 2-D woven SiC fibers exposed to nitrogen plasma is consistent with that of single fibers heat treated in static environments.

(2) Exposure to Oxidizing Plasmas

As shown in Fig. 7(a), a colorful iridescence pattern caused by optical interference was visually noticeable on the fabric surface after exposure to oxidizing plasmas, suggesting the presence of a vitreous silica layer. An SEM image in Fig. 7(b) confirms that SiC fibers undergo a dramatic change

in surface structure in oxidizing plasmas. The formation of a SiO₂ layer is supported by the corresponding EDS spectrum in Fig. 7(c), although surface oxidation was found to be nonuniform throughout the weave architecture. More importantly, morphological evidence of oxidation and silica deposits over 2 nm thick were easily observable after exposure times of only 60 s for temperatures above 1000°C. In contrast, silica formation in polycrystalline SiC is generally less pronounced when heated in molecular O₂ environment over the 1200°C–1500°C temperature range.²⁹ This salient feature allows us to conclude that abundant atomic oxygen in oxidizing plasmas, in conjunction with the greater surface area of the fabrics, could play a more damaging role than oxidation in static heating conditions.

Figure 8 shows that fiber oxidation in both air and oxygen plasmas leads to more severe strength reduction and embrittlement than nitrogen plasmas, as the time of exposure increases. Figure 8(a) displays a parabolic rate of embrittlement with a strength degradation attaining $\sim 1.3 \times 10^{-2}$ GPa/s over 240 s in the lead-ply coupon at 1325°C. In comparison, Takeda et al.⁷ reported a linear strength reduction of $\sim 6.5 \times 10^{-5}$ GPa/s in Hi-Nicalon fibers at 1400°C over a significantly longer time scale, 10 h. Therefore, a major finding of the present study is that exposure in air and oxygen plasmas leads to degradation rates up to 200 times higher than those reported for static heating at equivalent temperatures.

Strength reduction for the sub ply occurs at an initially slower rate compared to the lead-ply coupon, as shown in Fig. 8(b). Suppression of gas-surface interactions deeper within the weave likely contributes to this phenomenon, because boundary layer effects such as aerodynamic shear and dissociation fraction, may decrease within the weave architecture. Nevertheless, total strength loss at room temperature was manifest after 240 s from insertion for both lead-ply and sub-ply coupons, which shows a fundamentally different embrittlement behavior than that of woven SiC fibers treated in pure nitrogen plasma environment, Fig 6.

In parallel, an increase in fabric stiffness was observed when exposure times increased. Figure 7(b) proves that the increase in fabric stiffness results from interfilament adhesion within the tows. After initial oxidation, continuous surface iridescence change and little variation in silica volume within the weave architecture suggest further fusion of warp and weave tows by viscous silica flow. Consistent with the emission spectroscopy results, the extremely rapid temperature rise and silica formation from direct insertion into an oxidizing plasma flow could trap unreacted carbon underneath or within the silica layer. Trapped carbon is more likely to react

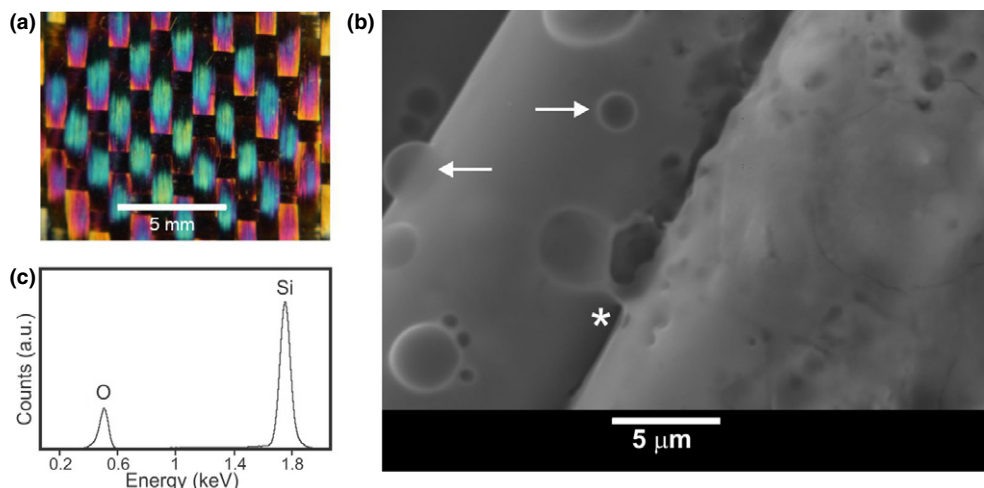


Fig. 7. Structure of 2-D woven SiC fabric after pure oxygen plasma exposure for 240 s. (a) Optical micrograph and (b) SEM image of the exposed lead-ply surface with arrows showing the formation of gas bubble at high temperature and a star for an example of surface bonding between two fibers. (c) EDS spectrum of the silica surface.

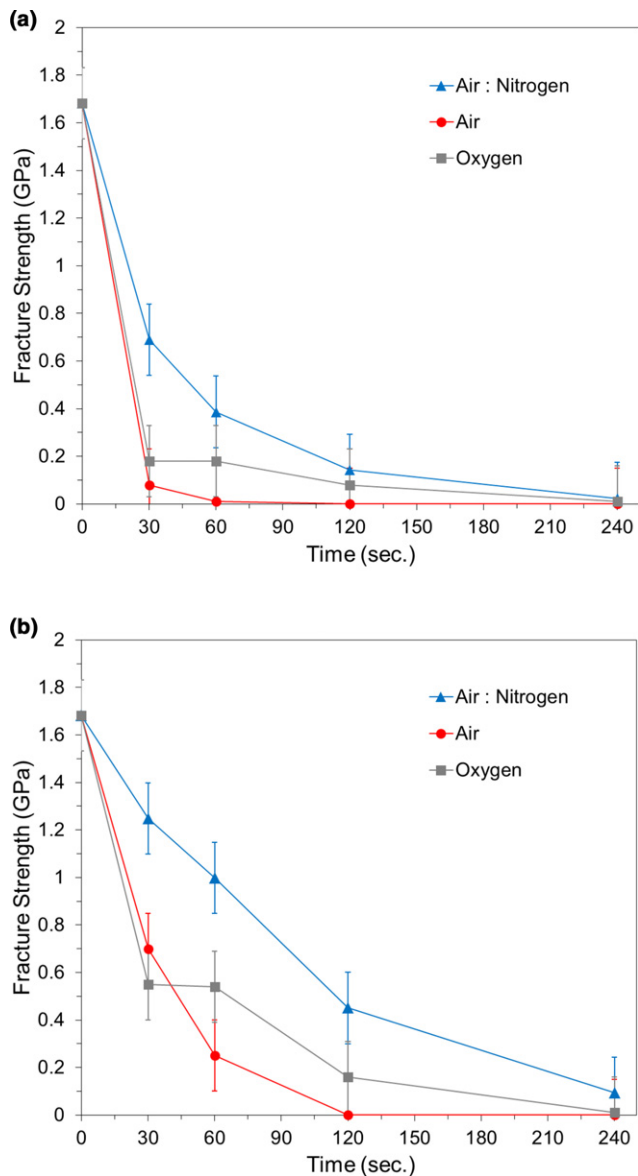


Fig. 8. Fracture strength after exposure to different oxidizing conditions for (a) lead-ply and (b) sub-ply coupons.

with oxygen atoms that diffuse through the silica and produce high CO pressures eventually leading to bubble formation, as shown in Fig. 7(b). In this study, it was observed that bubble formation increased with time and temperature of exposure, demonstrating the limited protective nature of the silica layer. A caveat, however, is that embrittlement in the silica and fabric material displayed at room temperature may not be relevant to flight conditions where it is more likely that a viscous silica layer is present. Nevertheless, isolated cracks in the highly oxidized sample can be seen in Fig. 7(b). No clear evidence of crack initiation at a single origin could be distinguished in SiC fibers exposed to oxidizing environment; however, the predominant embrittlement mechanism may be attributed to the microstructure defects in the oxide layer serving as crack nucleation sites. Moreover, Fig. 7(b) shows some evidence of surface bonding between fibers, which is related to the increase in fabric stiffness mentioned above.

Furthermore, any attempt to add oxygen to a steady nitrogen plasma always led to a passive silica coating or a form of oxy-nitridation. This discards the possible contribution of a destructively “active” oxidation regime that has been reported for extremely low oxygen partial pressures.⁸ In our experiments, the occurrence of temperature flares as

observed in Fig. 2, was actually found to continuously rise from no detectable minimum threshold, as the oxygen concentration was increased, suggesting that passive oxidation prevailed over active oxidation under all conditions of this study.

(3) Influence of Surface Temperature

In order to investigate the effects of surface temperature on fracture behavior in an oxidizing plasma, two-minute ICP tests were performed with an oxygen volume flow rate of 10 slpm at different power settings, see Table I. Admixtures with argon were used instead of nitrogen to broaden the achievable surface temperatures while maintaining a similar oxygen gas flow rate as for air plasma. The heat flux was varied from 26 to 107 W/cm², but it is clear that a concomitant change in gas chemistry occurred because the degree of O₂ dissociation increases with heat flux, until molecular oxygen becomes fully dissociated at high plasma temperatures.

Figure 9 shows the influence of surface temperature on the strength of Hi-Nicalon coupons exposed in oxygen-argon plasmas for 120 s. These tests show a gradual strength reduction up to 1533°C. We can observe a significant offset in tensile strength between the lead-ply and sub-ply coupons; however, the results between the two coupons at the same temperature are consistent with the hypothesis that gas-surface interactions diminish deeper within the weave. Also the strength difference between coupons is only evident below 1400°C, as any signs of protection of the sub-ply coupon by the lead-ply coupons disappear above this critical temperature.

IV. Conclusions

Fracture strength reduction and embrittlement in 2-D woven SiC fibers were studied through exposure of Hi-Nicalon SiC coupons in high-enthalpy dissociated oxygen, air and 100% nitrogen plasmas producing high surface temperatures, and tensile testing at room temperature. Microscopic analysis after exposure to nitrogen plasma showed little change in fiber morphology with only rare locations of fiber pitting from thermal decomposition that led to a moderate strength reduction of 50% within 30 s, compared to the strength of virgin fibers. In contrast, a major conclusion is that exposure to high oxygen atom concentration in air and oxygen plasmas results in a more severe embrittlement over shorter time scales, corresponding to degradation rates up to 200 times higher than those reported for static heating in conventional furnaces where only molecular oxygen is present. The origin of the accelerated embrittlement in oxidizing plasmas was found to be associated with the formation of a viscous silica

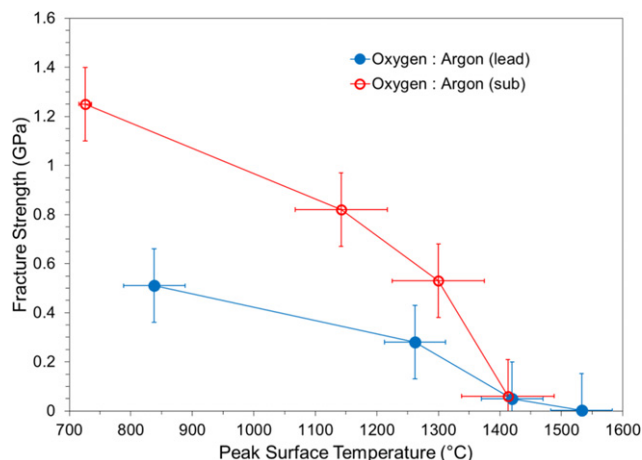


Fig. 9. Effect of surface temperature on fracture strength for lead-ply and sub-ply coupons exposed to different oxygen:argon plasma mixtures for 120 s.

surface layer leading to the development of gas bubbles, inter-filament adhesion, and critical flaws. Results obtained using admixtures of oxygen with argon to assess the influence of temperature suggested that the fracture resistance of 2-D woven SiC fibers is totally lost after 120 s of plasma exposure at 1400°C. The findings of this study have important implications for the deployment of new flexible ceramic materials for inflatable thermal protection systems currently in development at NASA, but further *in-situ* mechanical testing in plasma torch facility should be performed to fully understand the fracture mechanics of these materials at high temperature.

Acknowledgments

This work was performed under the auspices of NASA grant NNX12AL63G and AFOSR grant FA9550-11-1-0201 to DF and WO. FS and DM also gratefully acknowledge support for this work from NASA grant NNX14AN20A and the Vermont Space Grant Consortium.

References

- ¹J. A. Del Corso, F. M. Cheatwood, W. E. Bruce III, S. J. Hughes, and A. M. Calomino, "Advanced High-Temperature Flexible TPS for Inflatable Aerodynamic Decelerators"; AIAA 2011-2510, 21st AIAA Aerodynamic Decelerator Systems Technology Conference and Seminar, Dublin Ireland, May 23–26, 2011.
- ²G. Chollon, R. Pailler, R. Naslain, F. Laanani, M. Monthieux, and P. Olry, "Thermal Stability of a PCS-Derived SiC Fibre with a Low Oxygen Content (Hi-Nicalon)," *J. Mater. Sci.*, **32**, 327–47 (1997).
- ³J. A. DiCarlo and H. M. Yun, "Non-Oxide (Silicon Carbide) Fibers"; pp. 33–52 in *Handbook of Ceramic Composites*, Edited by N. Bansal. Springer, New York, 2005.
- ⁴P. M. Sawko and H. K. Tran, "Strength and Flexibility Properties of Advanced Ceramic Fabrics," *SAMPE Quarterly*, **17**, 7–13 (1985).
- ⁵T. Shimoo, K. Okamura, M. Ito, and M. Takeda, "High-Temperature Stability of Low Oxygen Silicon Carbide Fiber Heat-Treated Under Different Atmosphere," *J. Mater. Sci.*, **35**, 3733–9 (2000).
- ⁶H. M. Yun and J. A. DiCarlo, "Thermomechanical Behavior of Advanced SiC Fiber Multifilament Tows," *Ceram. Eng. Sci. Proc.*, **17A**, 61–7 (1996).
- ⁷M. Takeda, A. Urano, J.-I. Sakamoto, and Y. Imai, "Microstructure and Oxidative Degradation Behavior of Silicon Carbide Fiber Derived from Polycarbosilane," *J. Am. Ceram. Soc.*, **83** [5] 1171–6 (2000).
- ⁸T. Shimoo, K. Okamura, and Y. Morisada, "Active-to-Passive Oxidation Transition for Polycarbosilane-Derived Silicon Carbide Fibers Heated in Ar–O₂ Gas Mixtures," *J. Mater. Sci.*, **37**, 1793–800 (2002).
- ⁹J. J. Sha, T. Nozawa, J. S. Park, Y. Katoh, and A. Kohyama, "Effect of Heat Treatment on the Tensile Strength and Creep Resistance of Advanced SiC Fibers," *J. Nucl. Mater.*, **329–33**, 592–6 (2004).
- ¹⁰H. E. Kim and A. J. Moorhead, "Strength of Nicalon Silicon Carbide Fibers Exposed to High-Temperature Gaseous Environments," *J. Am. Ceram. Soc.*, **74**, 666–9 (1991).
- ¹¹H. K. Tran and P. M. Sawko, "Thermal Degradation Study of Silicon Carbide Threads Developed for Advanced Flexible Thermal Protection Systems," NASA Technical Memorandum 103952, August (1992).
- ¹²C. Vahlas, P. Bocabois, and C. Bernard, "Thermal Degradation Mechanisms of Nicalon Fiber: A Thermodynamic Simulation," *J. Mater. Sci.*, **29**, 5839–46 (1994).
- ¹³G. Emig and R. Wirth, "Tensile Strength of Silicon Carbide Bundles at Elevated Temperatures," *J. Mater. Sci.*, **30** [22] 5813–8 (1995).
- ¹⁴R. T. Bhatt and A. Garg, "Thermal Stability of Hi-Nicalon SiC Fiber in Nitrogen and Silicon Environments"; NASA Technical Memorandum 106987, Army Research Laboratory Technical Report ARL-TR-879, 10th International Conference on Composite Materials, August, 1995.
- ¹⁵N. Hochet, M. H. Berger, and A. R. Bunsell, "Microstructural Evolution of the Latest Generation of Small-Diameter SiC-Based Fibres Tested at High Temperatures," *J. Microsc.*, **185**, 243–58 (1997).
- ¹⁶Y. T. Zhu, S. T. Taylor, M. G. Stout, D. P. Butt, and T. C. Lowe, "Kinetics of Thermal, Passive Oxidation of Nicalon Fibers," *J. Am. Ceram. Soc.*, **81**, 655–60 (1998).
- ¹⁷M. D. Sacks, "Effect of Composition and Heat Treatment Conditions on the Tensile Strength and Creep Resistance of SiC-Based Fibers," *J. Eur. Ceram. Soc.*, **19**, 2305–15 (1999).
- ¹⁸G. He, T. Shibayama, and H. Takahashi, "Microstructural Evolution of Hi-NicalonTM SiC Fibers Annealed and Crept in Various Oxygen Partial Pressure Atmospheres," *J. Mater. Sci.*, **35**, 1153–64 (2000).
- ¹⁹T. Shimoo, F. Toyoda, and K. Okamura, "Thermal Stability of Low-Oxygen SiC Fiber (Hi-Nicalon) Subjected to Selected Oxidation Treatment," *J. Am. Ceram. Soc.*, **83** [6] 1450–6 (2000).
- ²⁰G. E. Youngblood, C. Lewinsohn, R. H. Jones, and H. Kohyama, "Tensile Strength and Fracture Surface Characterization of Hi-Nicalon SiC Fibres," *J. Nucl. Mater.*, **289**, 1–9 (2001).
- ²¹G. Kister and B. Harris, "Tensile Properties of Heat Treated Nicalon and Hi-Nicalon Fibers," *Composites: Part A, Appl. Sci. Manuf.*, **33**, 435–8 (2002).
- ²²S. W. Li, Z. D. Feng, H. Mei, and L. T. Zhang, "Mechanical and Microstructural Evolution of Hi-Nicalon Trade Mark SiC Fibers Annealed in O₂–H₂O–Ar Atmospheres," *Mater. Sci. Eng., A*, **487**, 424–30 (2008).
- ²³R. Yao, Z. Feng, L. Chen, Y. Zhang, and B. Zhang, "Oxidation Behavior of Hi-Nicalon SiC Monofilament Fibers in Air and O₂–H₂O–Ar Atmospheres," *Corros. Sci.*, **57**, 182–91 (2012).
- ²⁴M. Auweter-Kurtz, G. Hilfer, H. Habiger, K. Yamawaki, T. Yoshinaka, and H.-D. Speckmann, "Investigation of Oxidation Protected C/C Heat Shield Material in Different Plasma Wind Tunnels," *Acta Astronaut.*, **45** [2] 93–108 (1999).
- ²⁵COI Ceramics, "Hi-NicalonTM Ceramic Fiber"; ATK Space Systems. www.coiceramics.com. accessed on 11/08/2015.
- ²⁶J. Weiss, H. L. Lukas, J. Lorenz, G. Petzow, and H. Krieg, "Calculation of Heterogeneous Phase Equilibria in Oxide-Nitride-Systems: I. The Quaternary System C-Si-N-O," *Calphad*, **5**, 125–40 (1981).
- ²⁷H. Wada, M.-J. Wang, and T.-Y. Tien, "Stability of Phases in the Si-C-N-O System," *J. Am. Ceram. Soc.*, **71** [10] 837–40 (1988).
- ²⁸H. F. Schiefer, D. H. Taft, and J. W. Porter, "Effect of Number of Warp and Filling Yarns per Inch and Some Other Elements of Construction on the Properties of Cloth," *J. Res. Natl. Bur. Stand.*, **16**, 139–47 (1936).
- ²⁹J. A. Costello and R. E. Tressler, "Oxidation Kinetics of Silicon Carbide Crystals and Ceramics: I. In Dry Oxygen," *J. Am. Ceram. Soc.*, **69** [9] 674–81 (1986). □